Graphene Actively Mode-Locked Lasers

Jakub Bogusławski, Yadong Wang, Hui Xue, Xiaoxia Yang, Dong Mao, Xuetao Gan, Zhaoyu Ren, Jianlin Zhao, Qing Dai, Grzegorz Soboń, Jarosław Sotor, and Zhipei Sun**

Actively mode-locked lasers offer varying degrees of flexibility for a wider range of applications than their passively modulated counterparts, due to their capability for electrically controlled ultrahigh repetition rate operation. Graphene based electrooptic modulators with unique advantages of broad operation bandwidth and ultrafast speed are suitable for light modulation in various optoelectronic applications. Here, an actively mode-locked laser with a graphene based electrooptic modulator is reported for the first time. The active mode-locking technique combined together with the intracavity nonlinear pulse shortening effect allows the generation of transform-limited 1.44 ps pulses with pulse energy of 844 pJ. The electrically controlled repetition rate of generated pulses, a key performance advantage of active mode-locking, is also demonstrated. These results provide a practical and effective approach for actively mode-locked lasers with broad operation bandwidth and compact footprint, which contributes a new way for applications of two-dimensional (2D) layered materials in ultrafast lasers.

1. Introduction

Mode-locking is a method of choice to obtain ultrashort optical pulses, which has been widely used for a large range of applications, such as spectroscopy, industrial materials processing, and telecommunications.[1,2] Mode-locking methods can be generally classified as either active or passive. Passively mode-locked lasers usually operate at their fundamental repetition rate. While it is possible to increase the repetition rate using passive harmonic mode-locking,[3] it is normally very difficult to precisely control the harmonic number as they typically exhibit hysteresis phenomenon.[4] In contrast to passive mode-locking, active mode-locking allows the possibility to electrically control the output pulse repetition rate and thus pulse energy.[5,6] In addition, actively mode-locked lasers typically benefit from lower pump power threshold for pulse generation, as mode-locking operation does not rely on nonlinear optical effects that are commonly used in passive mode-locking (such as saturable absorption). However, actively mode-locked lasers normally need electrooptic modulators, which are typically fabricated with expensive and bulk materials, e.g., lithium niobate ($LiNbO_3$). These modulators also have some other limitations, like narrow operation bandwidth (from 10 to 100 nm, depending on the wavelength of operation and modulation principle), high insertion loss (≈3-7 dB) and large device footprint (e.g., ≈40 mm[7]). Therefore, new solutions enabling more compact, cost-effective and robust actively mode-locked lasers are of significant interest for high performance ultrafast pulse generation.

Dr. J. Bogusławski, Dr. G. Soboń, Prof. J. Sotor
Laser & Fiber Electronics Group
Faculty of Electronics
Wrocław University of Science and Technology
Wybrzeże S. Wyspiańskiego 27, 50-370 Wrocław, Poland
E-mail: Jakub.boguslawski@pwr.edu.pl

Dr. J. Bogusławski, Y. Wang, H. Xue, Prof. Z. Sun
Department of Electronics and Nanoengineering
Aalto University
Tietotie 3, 02150 Espoo, Finland
E-mail: Zhipei.sun@aalto.fi

Dr. J. Bogusławski
Institute of Physical Chemistry
Polish Academy of Sciences
Kasprzaka 44/52, 01-224 Warsaw, Poland

Y. Wang, Prof. D. Mao, Prof. X. Gan, Prof. J. Zhao
MOE Key Laboratory of Material Physics and Chemistry under Extraordinary Conditions, and Shaanxi Key Laboratory of Optical Information Technology
School of Science
Northwestern Polytechnical University
710072 Xi'an, P. R. China

Prof. X. Yang, Prof. Q. Dai
Division of Nanophotonics
CAS Center for Excellence in Nanoscience
National Center for Nanoscience and Technology
100190 Beijing, P. R. China

Prof. Z. Ren
State Key Lab Incubation Base of Photoelectric Technology and Functional Materials, and Institute of Photonics and Photon-Technology
Northwest University
710069 Xi'an, P. R. China

Prof. Z. Sun
QTF Centre of Excellence
Department of Applied Physics
Aalto University
FI-00076 Aalto, Finland

The ORCID identification number(s) for the author(s) of this article can be found under https://doi.org/10.1002/adfm.201801539.

DOI: 10.1002/adfm.201801539

Graphene electrooptic modulators (GEOM) could provide a promising opportunity to overcome the aforementioned issues of traditional bulk materials based modulators for active mode-locking, due to their performance advantages, such as broad operation bandwidth, low insertion loss, compact footprint, cost effectiveness, and easy integration.[8–17] Indeed, ref. [11] has demonstrated that GEOM can be used to actively Q-switch both Er- and Tm-doped fiber lasers, offering a broad operation bandwidth covering from 1.56 to 2 µm. Furthermore, using low-dimensional materials (including graphene) based electrooptic modulators not only enables superior performance, but also allows to make ultrafast lasers extremely compact. For example, easy integration of GEOMs into various optical systems (e.g., capacitors,[10–12] waveguide-,[8,13] or silicon photonic crystal nanocavity-integrated devices[14]) can make diverse laser design geometries possible. Graphene-based devices are also polarization insensitive, introduce small phase distortion and require lower drive voltage when compared with bulk $LiNbO_3$ modulators.[9] Despite the intensive research carried out on the design of various GEOMs,[8–15] thus far, graphene modulators have mainly been used for carrier-envelope offset control[18,19] and high-speed telecommunication.[15]

Here, we report for the first time an actively mode-locked ultrafast laser using a GEOM. The GEOM is designed and fabricated as a reflective multilayer structure with a dielectric layer placed between a mirror and graphene to increase the modulation depth at a low drive voltage (1.94% modulation depth with 10 V change). We use the GEOM to actively mode-lock an erbium-doped fiber laser with output pulse duration of 1.44 ps and pulse energy of 844 pJ at ≈1559 nm. Further, we demonstrate active harmonic mode-locking (HML) operation of the laser, which allows to electrically control the repetition rate of generated pulses.

2. Results and Discussion

2.1. Graphene Electrooptic Modulator Characterization

The schematic setup of the GEOM and its cross section are presented in **Figure 1**a,b, respectively. The modulator consists of a metal reflection bottom coating and monolayer graphene, which are separated by a high-k HfO_2 dielectric insulating layer (187 nm). The bottom contact and graphene are patterned into discs with 80 µm diameter. Raman spectrum of the transferred graphene layer is presented in Figure 1c. The spectrum contains pronounced 2D and G peaks, which confirms the presence of the monolayer graphene. The 2D peak exhibits a clear Lorentzian shape with a full width at half maximum (FWHM) of ≈29 cm^{-1}. The D band is also present and the D/G ratio is quite low (around 0.3). The appearance of the D peak is associated with defects formed during the transfer process. The microscope image of the fabricated GEOM is shown in the inset of Figure 1c. Details about the device fabrication are discussed in Experimental section. Note that our fabrication method allows multiple device fabrication on one chip, which can significantly reduce the device fabrication cost.

The thickness of the insulating layer is one of the key design parameters in our GEOM. In such a high reflectivity mirror formed by the bottom metal contact, the incoming and reflected waves form a standing wave at the surface. By changing the position of graphene layer along the standing wave, it is possible to control the linear absorption and thus modulation depth of the device. Indeed, careful adjustment of insulating layer thickness in our device can allow tailored linear absorption of graphene from almost 0% (when graphene is placed in the node) up to 9.2% (when placed precisely in the antinode of the standing wave, which corresponds to a $\lambda/4$ distance).[20] The absorption and electric field distribution in the device are designed using Fresnel transfer matrices method[21] for 1.55 µm wavelength at normal incidence. The refractive indices used during the device design are $3.292 + 1.915j$ for graphene (at zero voltage),[22] 2.07 for the HfO_2 layer, $0.524 + 10.74j$ for the gold layer, and $3.68 + 4.61j$ for the titanium layer. Here, the thickness of the HfO_2 layer is chosen to bring the graphene layer close to the antinode of the standing wave (see **Figure 2**a). The total insertion loss of the device is calculated to be 12.9%, from which 6.1% comes from the graphene layer (at zero voltage). The measured insertion loss of the device is 12.85% at zero voltage. It fits well with the theoretical design (Figure 2b).

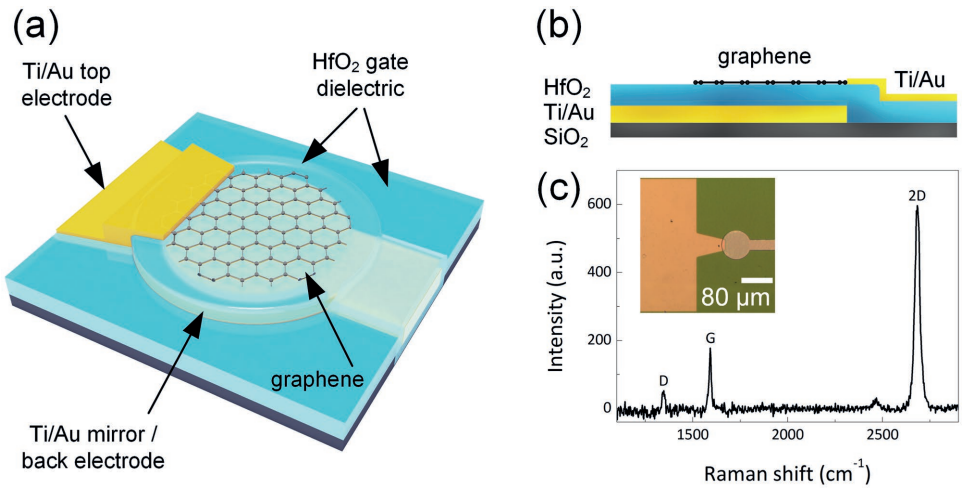

Figure 1. a) 3D schematic illustration and b) cross-section of the graphene modulator. c) Raman spectrum of the graphene layer after device fabrication. Inset: microscope image of the fabricated graphene device.

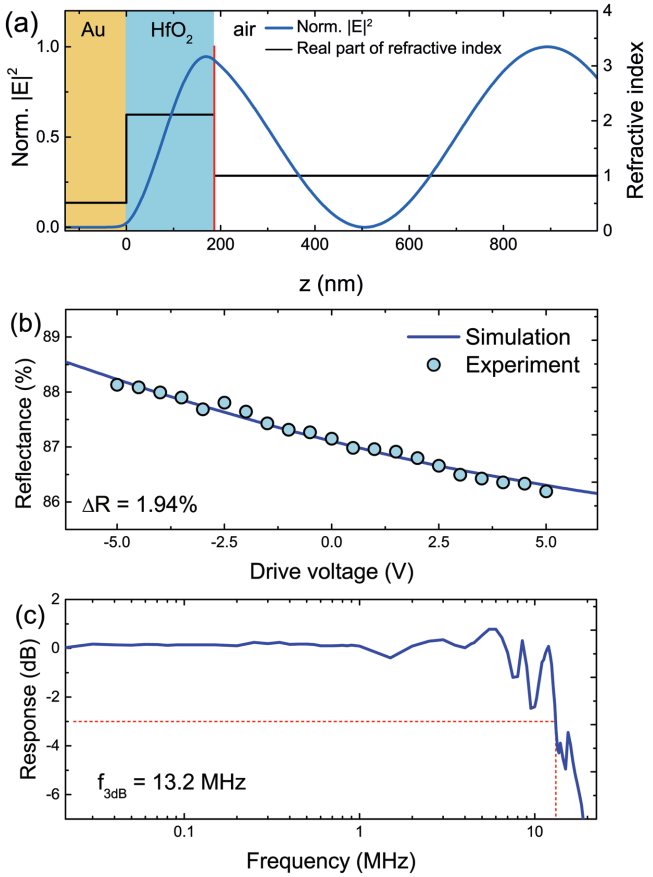

Figure 2. Characterization of the GEOM. a) Normalized electric field intensity calculation ($|E|^2$, blue line) and refractive index distribution (black lines) in the modulator. No voltage is applied. The wavelength is 1.55 µm. The red line indicates the position of the graphene layer. b) The reflectance of the GEOM at different gate voltages. c) Electrooptic frequency characteristic at 1.55 µm indicating a flat response with a 3 dB bandwidth ($f_{3\ dB}$) of ≈13.2 MHz.

Note that the position of the Dirac point in graphene is shifted at the zero voltage because of the predoping.[13] The reflectivity of the modulator may be further improved, e.g., by using a distributed Bragg reflector with higher reflectivity, but this typically comes with the price of narrow operation bandwidth.

When a voltage is applied to graphene, a change in charge-carrier density in graphene is created. This allows to shift Fermi level of graphene, and thus change its light absorption. To quantify the GEOM's modulation depth, we investigate its reflectivity under different drive voltages both experimentally and theoretically. The reflectance measurement is performed with a continuous wave (CW) laser diode at 1550 nm with 1 mW power. Figure 2b presents the measurement result. We obtain the modulation depth (ΔR) of 1.94%, when the voltage changes from −5 up to 5 V. For theoretical calculation we also use a Fresnel transfer matrix method with voltage-dependent values of complex refractive index of graphene. The optical absorption of graphene is proportional to its optical conductivity, which can be determined by Kubo formalism.[12,22,23] Complex refractive index can be derived from calculated optical conductivity.[22,24] We account for parameters of the dielectric material, which influence the charge density in the graphene layer. Offset voltage caused by natural doping is adjusted to obtain the best fit to experimental results, as in Ref. [22]. The simulation results agree well with the experimental data (Figure 2b), which confirms the operation principle of our GEOM.

The dynamic electrooptic response of the graphene modulator is investigated using the same CW laser diode and a radio frequency (RF) lock-in amplifier (Stanford, SR844) connected with a 22-GHz photodiode. Figure 2c presents the measurement result. The device exhibits a flat response with a 3 dB bandwidth of ≈13.2 MHz. The bandwidth is not limited by the carrier transit time of graphene, but may be limited by the parasitic response of the modulator. We estimate the capacitance of the device to be around 6 pF, as calculated from the parallel-plate model. Based on dynamic electrooptic response measurement, we can derive the resistivity of the RC circuit to be 2 kΩ. Part of this value (≈1 kΩ) arises from graphene sheet resistance and graphene/metal contact resistance; the remaining part can originate from defects in graphene created during the fabrication.

2.2. Graphene Actively Mode-Locked Laser

2.2.1. Fundamental Mode-Locking Operation

The GEOM is integrated with an Er-doped fiber laser working at 1.56 µm wavelength for active mode-locking. The experimental setup of the laser is presented in **Figure 3**. The basic layout of the laser cavity is described in the Experimental Section. First, we note that there is no passive mode-locking or Q-switching operation observed without an electrical signal applied to the modulator at any pump power or position of the polarization controller (PC). This proves that saturable absorption effect in graphene is insufficient to initiate and maintain pulse modulation. The active mode-locking operation occurs immediately when the modulating signal frequency is set to precisely match the roundtrip frequency of the laser cavity (f_0 = 4.3505725 MHz,

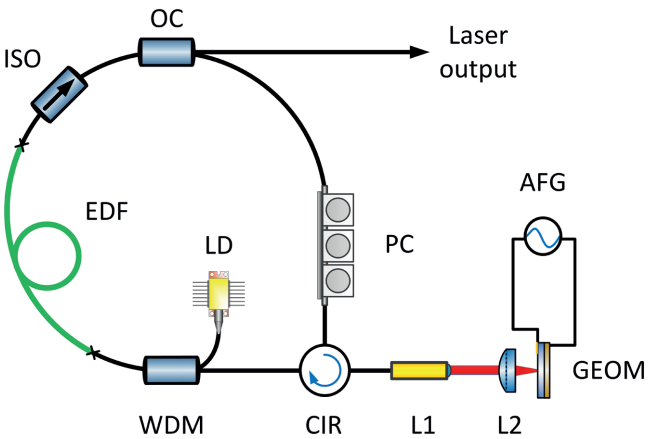

Figure 3. Experimental setup of the actively mode-locked laser. EDF: erbium-doped fiber; LD: laser diode; WDM: wavelength-division multiplexer; ISO: isolator; OC: output coupler; PC: polarization controller; CIR: circulator; L1: collimating lens; L2: focusing lens; AFG: arbitrary function generator.

see supplementary video) and the pump power exceeds the CW lasing threshold (18 mW). This is different from passive mode-locking operation,[25–30] in which the pulse generation threshold is typically larger than the lasing threshold. The amplitude of the modulating electrical signal is set to 8 V (from −4 to 4 V), where the best stability of the output laser pulses is observed. The mode-locking operation is lost after detuning the driving frequency by ≈100 Hz. This is because the active modulation frequency has to match well with the cavity roundtrip time for active mode-locking. Such a fundamental aspect is also observed in the passive mode-locking method, in which intracavity passive modulation frequency has to agree well with the cavity round trip time.[25–30] Stable pulses are generated regardless of PC setting; however, the PC could slightly adjust the output pulse duration by tuning intracavity polarization mode dispersion. The arbitrary function generator (AFG) allows generation of various electrical signals, including sine and square waves with a controlled filling factor. The mode-locking operation is possible with both signal shapes. However the best results (i.e., the shortest pulse) are observed using square wave with 10% filling factor. When using this shape of the electric signal, the modulator is "open" for a time period, which facilitates the ultrafast pulse formation (discussed below).

Stable mode-locking is obtained for a broad range of pump power starting from 18 up to 129 mW. For higher pump power the laser operation becomes unstable. The output power and pulse energy grow linearly together with the pump power (see **Figure 4**a). The highest output power is recorded to be 3.7 mW, which corresponds to pulse energy of 844 pJ. Detailed performance characterization (Figure 4b–e) is performed for the highest output power. The optical spectrum of generated pulses is presented in Figure 4b with a peak at 1559.2 nm. It has a shape typical for anomalous dispersion cavity (squared hyperbolic secant (sech^2) shape) with symmetric Kelly sidebands,[31] confirming soliton pulse operation. The FWHM is equal to 1.8 nm. A small CW component is present in the spectrum for all pumping powers. Further increase of modulation depth of the GEOM can remove the CW component. For comparison, the inset of Figure 4b presents the output spectrum of CW operation when no drive voltage is applied.

The autocorrelation trace of the output pulse is presented in Figure 4c together with sech^2 fit. The temporal width of the pulse is measured to be 1.44 ps. The peak power of the pulses at the laser output is estimated to be 516 W. Together with the output spectrum width, this gives the time-bandwidth (TBP) product of 0.32, indicating that output pulses are only slightly chirped. The obtained pulses are much shorter than Kuizenga–Siegman limit,[32] which sets the shortest duration of actively mode-locked pulses for given laser parameters. Here, we estimate it to be ≈480 ps in our case. However, it is possible to generate much shorter pulses in the presence of intracavity nonlinear pulse shortening effect (i.e., anomalous dispersion and self-phase modulation[33]) in fiber lasers. This causes a soliton-like pulse formation, which has a sech^2 shape, rather than a Gaussian profile (as typical for actively mode-locked lasers).[34] In our case, both optical spectrum and autocorrelation trace are well fitted with sech^2 function. Soliton pulse formation is further confirmed by the appearance of Kelly's

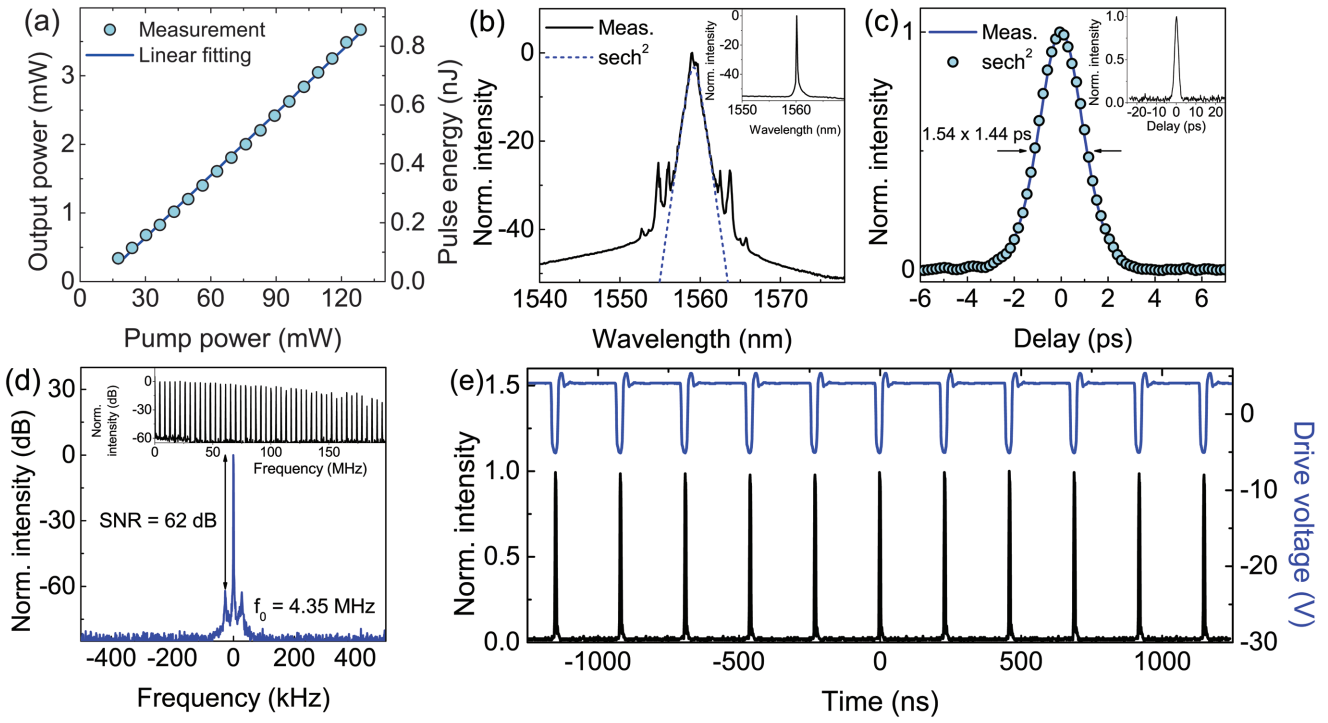

Figure 4. Fundamental mode-locking operation. a) Output power and pulse energy as a function of pump power. b) Optical spectrum with sech^2 fitting. Inset: CW output spectrum when no signal is applied to the GEOM. c) Autocorrelation trace of the output pulses. Inset: autocorrelation trace in a 50 ps span. d) RF spectrum at the fundamental frequency (f_0). Resolution bandwidth (RBW): 100 Hz. Inset: RF spectrum in a ≈200 MHz range, RBW: 30 kHz. e) Drive signal and synchronized output optical pulse train.

sidebands (Figure 4b) in the optical spectrum.[31] The output RF spectrum at 4.35 MHz fundamental frequency is presented in Figure 4d. The signal to noise ratio (SNR) is ≈62 dB. A broader spectrum of harmonics is presented in the inset of the figure. Note that the output pulses (Figure 4e) are well synchronized with the electrical signal, fully indicating high-quality active mode-locking. The pulse separation is 228 ns, which well corresponds to the fundamental repetition rate of the cavity. The output pulse train is very stable, which is characterized by excellent pulse-to-pulse amplitude stability (intensity fluctuations less than 1.4%). Worth noting that we do not observe any performance degradation of the GEOM during regular laser experiments within 1-year.

2.2.2. Harmonic Mode-Locking Operation

A major advantage of active mode-locking is its possibility to electrically control the repetition frequency of the generated pulses. This can be done by taking advantage of harmonic mode-locking. To do so, we increase the modulation signal frequency to 8.7012 MHz, which corresponds to second harmonic of the laser cavity. The amplitude of modulating signal is kept at the same level. Similarly to the fundamental operation, the mode-locking operation occurs immediately after reaching the CW lasing pump threshold (**Figure 5**a); however, the operation is unstable for lower pumping powers and stabilizes at around 60 mW. The highest output power and energy at stable operation are equal to 3.8 mW and 437 pJ, respectively (at a pump power of 129 mW). The optical spectrum of the output pulses is centered at 1559.3 nm (Figure 5b) with 1.82 nm FWHM. The CW component is visible in the spectrum irrespective of pumping power. The output spectrum also has a clear soliton shape with distinct Kelly's sidebands.

The recorded autocorrelation trace gives 1.57 ps pulse duration, assuming a sech^2 shape (Figure 5c). The single pulse operation with no pre- or postpulses is confirmed by the measurement performed with a 50 ps scan range (inset of the figure). The generated pulses are slightly chirped with the TBP of 0.34. The fundamental beat note of second harmonic operation (f_0 = 8.7012 MHz) is presented in Figure 5d. The SNR is equal to 66 dB. The inset of the figure shows the electrical spectrum recorded in a 25 MHz range. The supermode suppression is 34 dB at 8.7 MHz beat note, and 17 dB at 17.4 MHz. The second harmonic operation is further confirmed by recording the output pulse train on the oscilloscope (Figure 5e). The pulse-to-pulse temporal separation is 114 ns, which corresponds to 8.7 MHz repetition rate. There is a slight amplitude modulation in the pulse train. Harmonically generated second pulse has lower amplitude, which might be a consequence of insufficient modulation depth of the GEOM. When the GEOM is modulated with third and fourth harmonic frequency, i.e., 13.05 and 17.4 MHz, the generated pulse train tends to be unstable. This can be explained by the slow electrooptic response of our GEOM after reaching the 3 dB frequency (i.e., 13.2 MHz). No pulsed operation is observed for higher harmonic modulating frequencies. But we believe faster graphene modulators will allow operation with

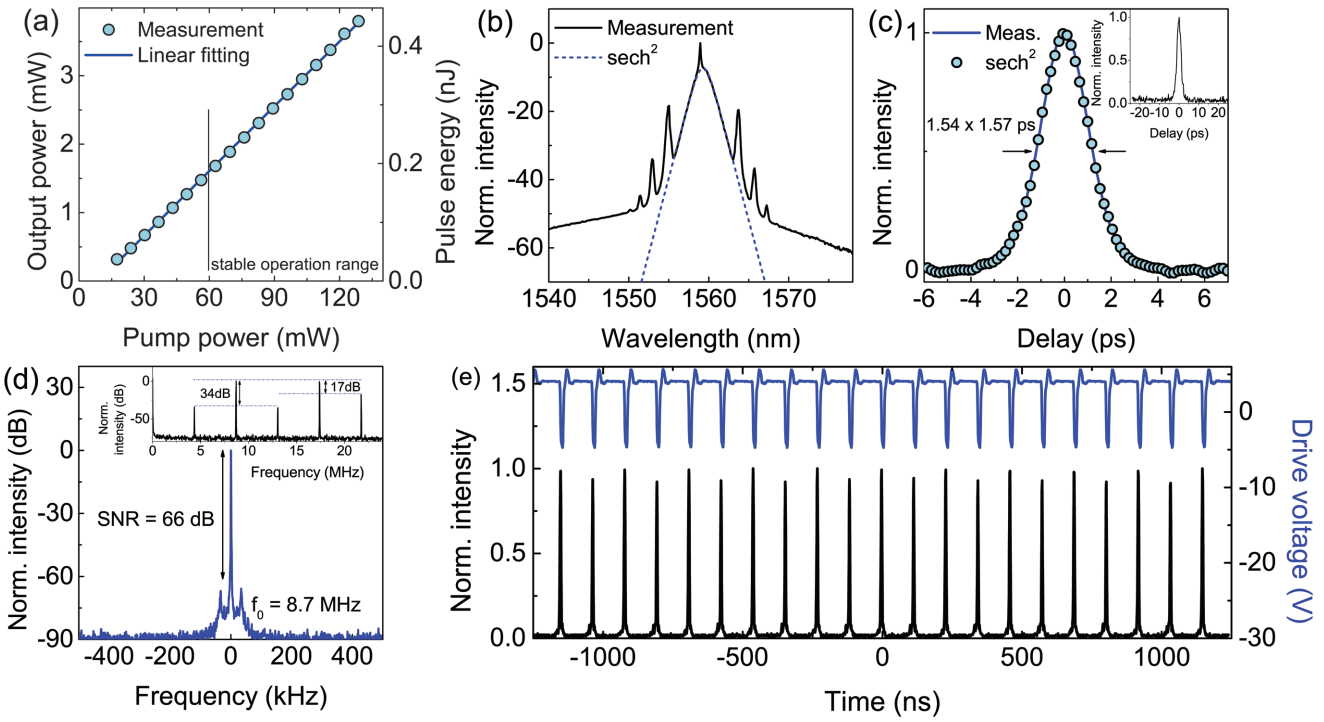

Figure 5. Harmonic mode-locking operation. a) Output power and pulse energy as a function of pump power. b) Optical spectrum with sech^2 fitting. c) Autocorrelation trace of output pulses. Inset: autocorrelation trace in a 50 ps span. d) RF spectrum at the output repetition rate of the laser (f_0). RBW: 100 Hz. Inset: RF spectrum in a 25 MHz range, RBW: 30 kHz. e) Drive voltage trace and synchronized output pulse train.

higher order of harmonics (e.g., >1 GHz output frequency, or even higher).

3. Conclusion

In conclusion, we have demonstrated for the first time a graphene electrooptic modulator based actively mode-locked laser. The modulator is designed as a simple and multilayer structure with graphene working as an active layer. Using only monolayer graphene, the ≈2% modulation depth at a low drive voltage with a modulation speed in the megahertz range is achieved. This allows for electrically controlled picosecond pulse generation with the energy of 844 pJ at ≈1559 nm. The harmonic mode-locking operation is also demonstrated. It is important to highlight that the presented device provides the design freedom, which will allow further optimization of modulator's parameters, e.g., modulation speed toward a GHz range. Our results provide a simple, robust and viable approach to active mode-locking of lasers for various scientific and industrial applications.

4. Experimental Section

Graphene Electrooptic Modulator Fabrication: The bottom metal reflection coating (i.e., Ti/Au, 5/130 nm thickness) was first deposited on SiO_2/Si substrate and patterned into an 80 µm diameter disk via conventional electron beam lithography (EBL). Atomic layer deposition (ALD) process was then used to deposit HfO_2 (187 nm thickness) on the patterned metal contact, acting as a high permittivity dielectric layer. Next, monolayer chemical vapor deposition (CVD) grown graphene was transferred onto the HfO_2 insulating layer (see Figure 1b) by using the method described in ref. [35]. The graphene sheet was subsequently patterned into an 80 µm disk with EBL and reactive ion etching process. Finally, metal titanium/gold (5/50 nm thickness) contact was fabricated on the top of graphene for gating.

Ultrafast Laser Experimental Setup: The gain medium of the laser was ≈80 cm long erbium-doped fiber (EDF). The laser was forward-pumped by a 980 nm laser diode (LD) coupled into the cavity through a 980/1550 wavelength-division multiplexer (WDM). The polarization-independent isolator (ISO) ensured clockwise, unidirectional operation, providing higher isolation than a circulator (CIR). The 10% output coupler (OC) extracted the radiation outside the cavity for measurements. The polarization controller (PC) was included to adjust the intracavity polarization state. The GEOM was inserted in a linear part of the cavity coupled with the ring-shaped part by a fiber circulator. A fiber collimator (L1) and an aspheric focusing lens (f = ≈4.6 mm, L2) were used to extract the beam outside the fiber and focus on the surface of the GEOM. The beam size at the focal point was ≈18.6 µm. The total cavity length was ≈47.6 m, which corresponded to ≈4.35 MHz fundamental repetition rate. The net cavity dispersion was anomalous and equal to ≈−1.094 ps^2. An electrical signal was generated using an arbitrary function generator (Tektronix AFG3252, AFG) to drive the GEOM.

Laser Characterization: The laser output was monitored using an optical spectrum analyzer (Anritsu, MS9740A), a RF signal analyzer (Anritsu, MS2692A), a digital oscilloscope (Tektronix, TDS2024C) connected to a fast photodiode (Discovery, DSC2-30S), and an optical autocorrelator (APE, PulseCheck).

Supporting Information

Supporting Information is available from the Wiley Online Library or from the author.

Acknowledgements

J.B. and Y.W. contributed equally to this work. This research was supported by the Academy of Finland (276376, 284548, 295777, 304666, 312297, 312551, 314810); TEKES (OPEC); the European Union's Seventh Framework Program (No. 631610); China Scholarship Council; the International Science and Technology Cooperation Project of China (No. 2014DFR10780); Chair of Electromagnetic Field Theory, Electronic Circuits and Optoelectronics, Wrocław University of Science and Technology (statutory funds). The authors also acknowledge the provision of technical facilities of the Micronova, Nanofabrication Centre of Aalto University. An author (Jakub Bogusławski) received financial support for preparation of Ph.D. thesis from Polish National Science Centre in a frame of doctoral scholarship (UMO-2016/20/T/ST7/00189).

Conflict of Interest

The authors declare no conflict of interest.

Keywords

electrooptic materials, graphene, mode-locked lasers, photonics

Received: February 28, 2018
Revised: April 10, 2018
Published online: May 29, 2018

[1] U. Keller, *Nature* **2003**, *424*, 831.
[2] M. E. Fermann, A. Galvanauskas, G. Sucha, *Ultrafast Lasers: Technology and Applications*, CRC Press, New York **2002**.
[3] A. Grudinin, S. Gray, *J. Opt. Soc. Am. B* **1997**, *14*, 144.
[4] A. Komarov, H. Leblond, F. Sanchez, *Phys. Rev. A* **2005**, *71*, 053809.
[5] H. A. Haus, *IEEE J. Sel. Top. Quantum Electron.* **2000**, *6*, 1173.
[6] K. Sarwar Abedin, N. Onodera, M. Hyodo, *Appl. Phys. Lett.* **1998**, *73*, 1311.
[7] E. L. Wooten, K. M. Kissa, A. Yi-Yan, E. J. Murphy, D. A. Lafaw, P. F. Hallemeier, D. Maack, D. V. Attanasio, D. J. Fritz, G. J. McBrien, D. E. Bossi, *IEEE J. Sel. Top. Quantum Electron.* **2000**, *6*, 69.
[8] M. Liu, X. Yin, E. Ulin-Avila, B. Geng, T. Zentgraf, L. Ju, F. Wang, X. Zhang, *Nature* **2011**, *474*, 64.
[9] Z. Sun, A. Martinez, F. Wang, *Nat. Photonics* **2016**, *10*, 227.
[10] E. O. Polat, C. Kocabas, *Nano Lett.* **2013**, *13*, 5851.
[11] D. Li, H. Xue, M. Qi, Y. Wang, S. Aksimsek, N. Chekurov, W. Kim, C. Li, J. Riikonen, F. Ye, Q. Dai, Z. Ren, J. Bai, T. Hasan, H. Lipsanen, Z. Sun, *2D Mater.* **2017**, *4*, 025095.
[12] C.-C. Lee, S. Suzuki, W. Xie, T. Schibli, *Opt. Express* **2012**, *20*, 5264.
[13] M. Liu, X. Yin, X. Zhang, *Nano Lett.* **2012**, *12*, 1482.
[14] Y. Gao, R.-J. Shiue, X. Gan, L. Li, C. Peng, I. Meric, L. Wang, A. Szep, D. Walker Jr., J. Hone, D. Englund, *Nano Lett.* **2015**, *15*, 2001.
[15] C. T. Phare, Y.-H. D. Lee, J. Cardenas, M. Lipson, *Nat. Photonics* **2015**, *9*, 511.
[16] E. J. Lee, S. Y. Choi, H. Jeong, N. H. Park, W. Yim, M. H. Kim, J.-K. Park, S. Son, S. Bae, S. J. Kim, K. Lee, Y. H. Ahn, K. J. Ahn, B. H. Hong, J.-Y. Park, F. Rotermund, D.-I. Yeom, *Nat. Commun.* **2015**, *6*, 6851.
[17] A. Autere, H. Jussila, Y. Dai, Y. Wang, H. Lipsanen, Z. Sun, *Adv. Mater.* **2018**, *30*, 1705963.
[18] C.-C. Lee, C. Mohr, J. Bethge, S. Suzuki, M. Fermann, I. Hartl, T. Schibli, *Opt. Lett.* **2012**, *37*, 3084.
[19] N. Kuse, C.-C. Lee, J. Jiang, C. Mohr, T. Schibli, M. Fermann, *Opt. Express* **2015**, *23*, 24342.

[20] C. Zaugg, Z. Sun, V. Wittwer, D. Popa, S. Milana, T. Kulmala, R. Sundaram, M. Mangold, O. Sieber, M. Golling, Y. Lee, J. H. Ahn, A. C. Ferrari, U. Keller, *Opt. Express* **2013**, *21*, 31548.
[21] S. J. Byrnes, *Multilayer optical calculations*, arXiv:1603.02720, **2016**, https://arxiv.org/abs/1603.02720.
[22] F. Xu, S. Das, Y. Gong, Q. Liu, H.-C. Chien, H.-Y. Chiu, J. Wu, R. Hui, *Appl. Phys. Lett.* **2015**, *106*, 031109.
[23] C. Xu, Y. Jin, L. Yang, J. Yang, X. Jiang, *Opt. Express* **2012**, *20*, 22398.
[24] J. Gosciniak, D. T. Tan, *Sci. Rep.* **2013**, *3*, 1897.
[25] Z. Sun, T. Hasan, A. C. Ferrari, *Physica E* **2012**, *44*, 1082.
[26] A. Martinez, Z. Sun, *Nat. Photonics* **2013**, *7*, 842.
[27] Z. Sun, T. Hasan, F. Torrisi, D. Popa, G. Privitera, F. Wang, F. Bonaccorso, D. M. Basko, A. C. Ferrari, *ACS Nano* **2010**, *4*, 803.
[28] T. Hasan, Z. Sun, F. Wang, F. Bonaccorso, P. H. Tan, A. G. Rozhin, A. C. Ferrari, *Adv. Mater.* **2009**, *21*, 3874.
[29] Q. Bao, H. Zhang, Y. Wang, Z. Ni, Y. Yan, Z. X. Shen, K. P. Loh, D. Y. Tang, *Adv. Funct. Mater.* **2009**, *19*, 3077.
[30] H. Zhang, D. Y. Tang, L. M. Zhao, Q. L. Bao, K. P. Loh, *Opt. Express* **2009**, *17*, 17630.
[31] S. Kelly, *Electron. Lett.* **1992**, *28*, 806.
[32] D. Kuizenga, A. Siegman, *IEEE J. Quantum Electron.* **1970**, *6*, 694.
[33] F. Kärtner, D. Kopf, U. Keller, *J. Opt. Soc. Am. B* **1995**, *12*, 486.
[34] T. F. Carruthers, I. N. Duling, *Opt. Lett.* **1996**, *21*, 1927.
[35] J. W. Suk, A. Kitt, C. W. Magnuson, Y. Hao, S. Ahmed, J. An, A. K. Swan, B. B. Goldberg, R. S. Ruoff, *ACS Nano* **2011**, *5*, 6916.

